Chaotic itinerancy generated by coupling of Milnor attractors

Ichiro Tsuda and Toshiya Umemura
Department of Mathematics, Graduate School of Science, Hokkaido University, Sapporo, 060-0810, Japan

Abstract

We report the existence of chaotic itinerancy in a coupled Milnor attractor system. The attractor ruins consist of tori or local chaos generated from the original Milnor attractors. The chaotic behavior exhibited by a single orbit can be considered a "non-stationary" state, due to the extremely slow convergence of the Lyapunov exponents, but the behavior averaged over randomly chosen initial conditions is consistent with the limit theorem. We present as a possibly new indication of chaotic itinerancy the presence of slow decay of large fluctuations of the largest Lyapunov exponent.

A typical characteristic of chaos is the sensitive dependence on initial conditions that is measured by the Lyapunov exponent. The presence of positive Lyapunov exponent is, however, insufficient to characterize chaotic itinerancy. We investigated the fluctuations and convergence of the exponents.

1 Introduction

The concept of chaotic itinerancy (CI) was proposed [1, 2, 3] to describe the curious transitory dynamics, such as chaotic transitions, observed to take place between the ruins of attractors in various dynamical systems. In three representative works treating CI, Ikeda studied a dynamical system consisting of delay-differential equations, Kaneko studied globally coupled maps (GCM), and Tsuda studied a dynamical system consisting of non-equilibrium neural networks. Among such systems, GCMs have been most thoroughly studied, because they possess a symmetry that is absent in the other two types of systems. In his GCM, Kaneko [4] obtained a description of the mechanism underlying CI in terms of Milnor attractors, and he also investigated the occurrence of CI through saddle-node bifurcations. In that system, at the critical parameter value in the saddle and node merging, Milnor attractors appear, and after the collapse of these Milnor attractors, the system exhibits CI moving among the ruins of Milnor attractors, where each Milnor attractor represents a type of synchronized chaotic cluster. The presence of such synchronized chaos in GCM results from the chaos exhibited by the uncoupled individual maps. Such synchronized chaos defines an invariant subspace. In such a case, in which

the system possesses symmetry under certain group actions, like transposition of the individual maps, it is easily proved that a set that is invariant under such group action is also invariant under the system dynamics. The presence of riddled basins is related to the existence of transitory orbits between invariant sets.

While some progress has been made in the elucidation of the mechanism underlying CI, it has not yet been fully clarified. Moreover, the relation between the occurrence of CI and the presence of riddled basins is not clear. Actually, there has yet been no observation of a riddled basin in non-equilibrium neural networks. In order to clarify the mechanisms underlying CI and its relation to basin structure, we study here chaotic transitions that differ from those observed in system with invariant sets whose existence is due to a simple symmetry like those mentioned above. We consider a system consisting of coupled circle maps, with individual map possessing a Milnor attractor. We investigate the nature of the dynamic behavior of this coupled system, whose couplings depend on the relative phase angles of the individual maps. Our model does possess a type of symmetry, but this symmetry is not directly related to the appearance of chaotic transitions. Because of this more complicated type of symmetry, in our system, it is not the Milnor attractors of the individual maps but a torus generated by interactions between such Milnor attractors that results in an attractor ruin after crisis.

We found a complicated basin structure consisting of a riddled area and Wada basin-like area, but we did not recognize the well-defined relation between the presence of riddled basin and the appearance of CI via the appearance of Milnor attractors. On the other hand, we found the large fluctuations and slow convergence of the Lyapunov exponents. It is well known that one of the main characteristics of deterministic chaos is the presence of positive Lyapunov exponents. On the other hand, we assert, in this paper, that the large fluctuations and slow convergence of even the largest Lyapunov exponent can be a typical indication of the presence of CI.

The organization of the paper is as follows. In §2, we describe the model. We demonstrate the existence of chaotic itinerancy between ruins of tori in §3 and transient chaotic itinerancy between ruins of local chaos in §4. In §5, we describe the statistical character of chaotic itinerancy in the system we study. We treat the time development of transients of the Lyapunov exponents and their statistics in relation with ergodicity. Section 6 is devoted to a conclusion and discussion with a new hypothesis.

2 The model

The system we consider in this paper consists of coupled maps, each of which is given by

$$x_{n+1} = f(x_n) \quad (mod 1), \tag{1}$$

$$f(x) \quad = \quad x - \omega cos(2\pi x) + \omega, \tag{2}$$

where n represents a discrete time, which takes natural number values, and ω $(0 < \omega < 1)$ is a parameter that determines a degree of nonlinearity. This map is called a circle map. Only the difference from the conventional use is that the parameter ω is introduced to control both the terms of nonlinearity and shift. By this use of the parameter, all the fixed points become indifferent fixed points whose stability is neutral.

Conventional attractors are defined geometrically, using the concept of attracting sets. According to this definition, roughly speaking, an attractor is a set of points with the property that all points in its neighborhood either approach it or are absorbed into it as the system evolves. Milnor (1985) [5] defined an attractor from another viewpoint, in which both topological and measure-theoretic concepts play roles. We now consider this definition. Let ρ be a measure equivalent to the Lebesgue measure on a metric space X, on which dynamical flows are defined. A compact invariant set α is called a (minimal) Milnor attractor if the following hold:

1. The basin of attraction $B(\alpha)$ of α has a positive ρ-measure, *i.e.* $\rho(B(\alpha)) > 0$.
2. There does not exist a proper closed subset α' satisfying $\rho(B(\alpha) \backslash B(\alpha')) = 0$.

According to this definition, a Milnor attractor can possess an unstable manifold. The dynamical system (1) is critical in the sense that $x = 0$ is a fixed point of this map and a Milnor attractor for any value of ω (see Fig.1). When ω is small, $x = 0$ is the unique fixed point, as is seen in Fig.1 (a), but when $\omega = 1/2$, $x = 1/2$ becomes another fixed point and a Milnor attractor. This situation is depicted in Fig.1 (b).

In the present paper, we consider the following system of coupled maps defined on a circle:

$$x_{n+1}(i) = f(x_n(i)) + \epsilon(sin(2\pi x_n(i-1)) + sin(2\pi x_n(i+1)) - 2sin(2\pi x_n(i))), \tag{3}$$
$$(i = 1, 2, \cdots, N).$$

Here, N is the dimension of the system, and ϵ is a coupling constant that takes a non-negative real number value. For any n, $x_n(0)$ and $x_n(N+1)$ are defined as $x_n(N)$ and $x_n(1)$, respectively. Thus the present system is a coupled map lattice (CML) with a circle map [6] consisting of Milnor attractor(s).

3 Observation of CI through tori

We first consider (3) in the case $N = 5$. This case has a special interest since it is an intermediate case between CML and GCM. Let us consider the simple but typical case such that all the connection strengths are identical. GCM possesses the permutation symmetry. In other words, GCM is invariant under permutation over all elementary

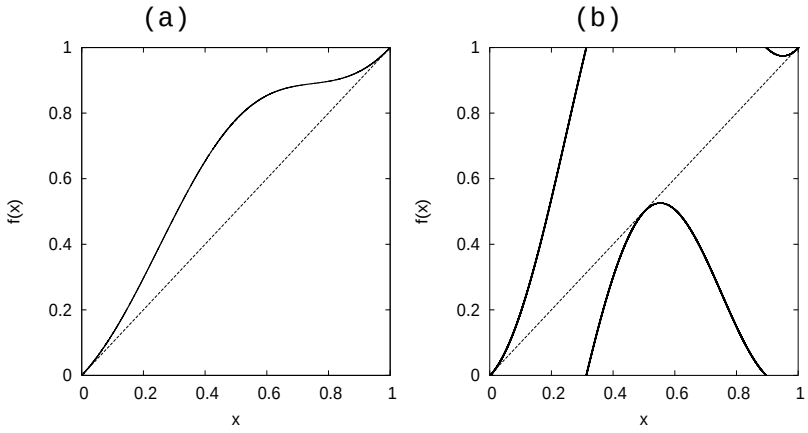

Figure 1: The individual map of the system studied in the case of critical conditions. (a) $\omega = 0.14$. Here, the origin is the only indifferent fixed point. (b) $\omega = 0.5$. Here there are two indifferent fixed points. The indifferent fixed points depicted in both (a) and (b) are Milnor attractors. The individual maps used in the coupled system in this paper correspond to (b).

individual maps. When this group action commutes with the dynamical system defined by GCM, the the permutation symmetry leads the existence of invariant subspace. On the other hand, CML on a circle does not possess such symmetry but possesses the translational symmetry. Because the translation is a special case of the permutation, CML is less symmetric than GCM. The difference of dynamics between CML and GCM can be characterized by the difference of a total number of connections. Let the total number of connections in CML defined on a circle and GCM, both having N elementary individual maps be denoted by $CML(N)$ and $GCM(N)$, respectively. One way of quantification of such a difference is to define the following quantity denoted by $Q(N)$:

$$Q(N) := (GCM(N) - CML(N))/GCM(N). \tag{4}$$

The CML and the GCM are equivalent in both cases of $N = 2$ and $N = 3$, that leads $Q(2) = Q(3) = 0$. In the limit $N \to \infty$, we obtain $Q(\infty) = 1$. In the intermediate cases, we easily see, for instance, $Q(4) = 1/3, Q(5) = 1/2$ and $Q(6) = 3/5$. In such a way, an equal effect of CML and GCM to the dynamics can be expected in the case of $N = 5$. In GCM, a typical CI has been found [2] and widely investigated, [6] whereas in CML it is known that CI-like transitory dynamics are rare. One of reasons may lie on the less symmetry in CML than in GCM. By this reason, the study of CML on a circle with $N = 5$ is important. For the comparison, we also study in §4 the case of $N = 10$ that is more CML-like since $Q(10) = 7/9$.

In Fig. 2, we display its bifurcation diagram with respect to ϵ for a fixed $\omega = 1/2$ and $N = 5$. In this figure there is one orbit for each value of ϵ, and the same initial conditions were used for each. As seen below, this system has multiple basins, and hence the bifurcation diagram depends on the initial conditions.

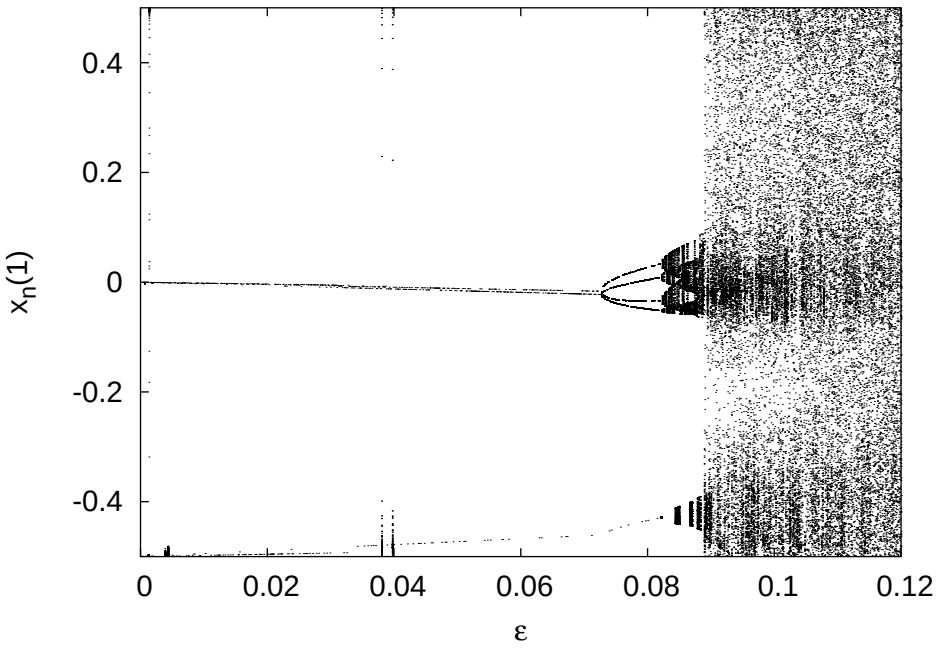

Figure 2: Bifurcation diagram projected onto $x(1)$ in the case $\omega = 0.5$ and $N = 5$. Identical initial conditions were used for all parameter values of ϵ. Because many attractors coexist in this type of coupled system, the nature of the diagram depends on the initial conditions.

Several kinds of CI are found for some parameter values, one of which appears near $\epsilon = 0.08885$, where five one-dimensional tori are still stable. These tori are identical in the sense that they differ only by the labeling of the variables. Figure 3 displays the dynamic behavior and the attractor of one of these tori for $\epsilon = 0.08885$. In Fig.3(a) a typical time series of the system is displayed, where the individual time series of each of five variables are plotted together. Two pairs of variables, $x(1)$ with $x(2)$, and $x(3)$ with $x(5)$, are almost synchronized in one phase and are apparently desynchronized in another phase. In the phase with quasi-synchronization, a fine structure is observed (see the oblique part of the torus in Fig. 3(b)). The fine structure caused by a small difference between $x(1)$ and $x(2)$ and between $x(3)$ and $x(5)$ eventually grows, and the dynamics of the individual variables thereby become completely desynchronized. In this range of parameter values, periodic orbits coexist, but their basins of attraction are extremely small, and moreover these periodic orbits play no role in the occurrence of CI.

The CI exhibited in this case appears soon after the collapse of the tori via crisis. As seen in Fig. 4, the orbit is trapped in the region where a torus existed, tracing the ruin of torus and then is kicked out of this region and behaves chaotically. Two such states of tracing appear, which we call the "up-state" and the "down-state." This is seen in Fig.4(a). The "up-state" is that in which the orbit traces the ruins of tori denoted T1, T3, T4 and T5, and the "down-state" that in which it traces the ruin of the torus denoted

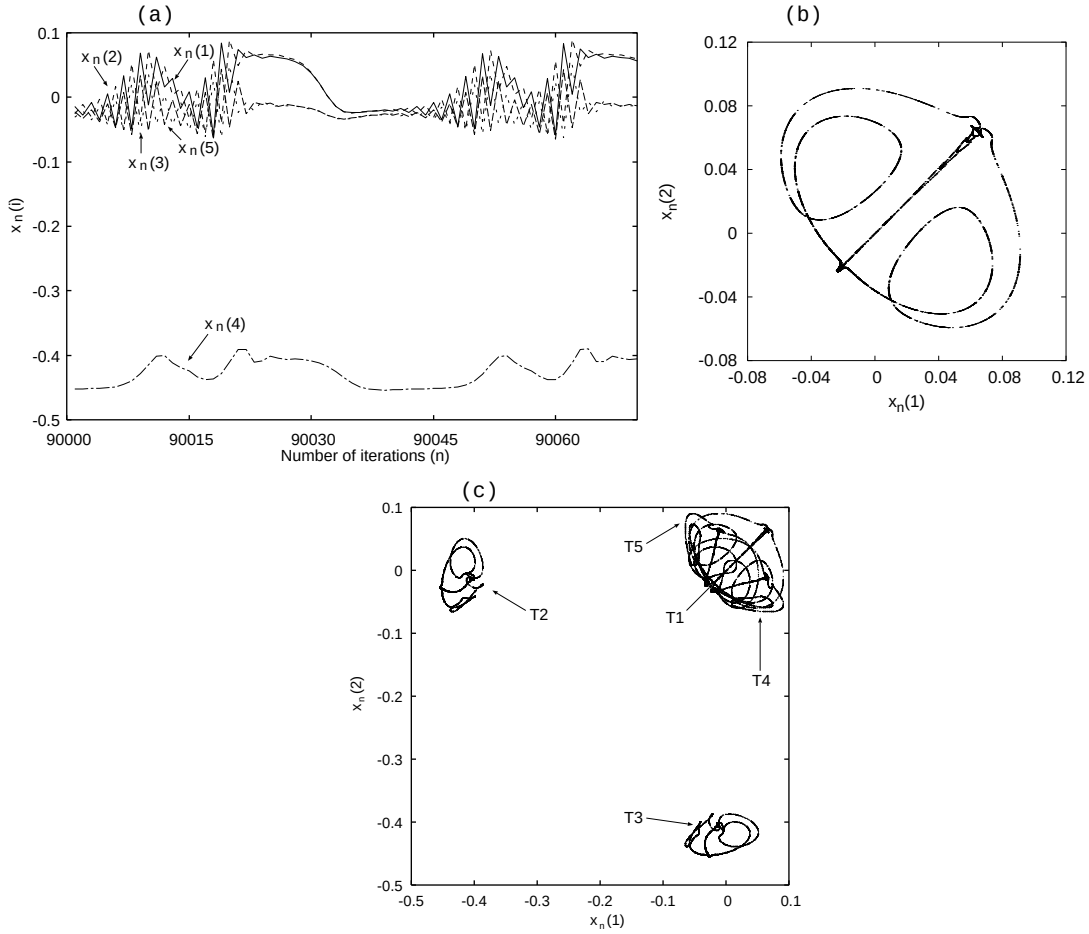

Figure 3: (a) Overlaid time series of five tori. (b) Phase portrait of a certain torus in $x(1) - x(2)$ space. (c) Overall phase portrait of five tori in $x(1) - x(2)$ space. Here, $N = 5, \omega = 0.5$, and $\epsilon = 0.08885$.

$T2$. Moreover, in this case ($\epsilon = 0.088858$), there are two positive Lyapunov exponents, and the Lyapunov dimension is estimated as 4.03. However, as discussed below, there is a serious difficulty involved in the computation of the Lyapunov exponents, and for this reason, this estimation of the dimensionality is not reliable.

Because the transient motion of tori is similar to CI, it is natural to think that the appearance of CI must be deeply related to some instability of tori. In order to clarify the mechanism underlying the destabilization of tori and its role in the appearance of CI, we studied the stability of tori with respect to perturbations. The basins of attraction of the five tori have peculiar structures. The graphs obtained by investigating the basin structures of all tori are similar. We found that the basin of each torus consists of a combination of a riddled structure and a Wada basin-like structure [8].

Following Kaneko [7], we calculated the probabilities of orbits jumping out of tori when a perturbation is applied to the tori. In Fig.5, this probability is plotted for T1 as a function of the strength of the perturbation. Perturbations were applied to many

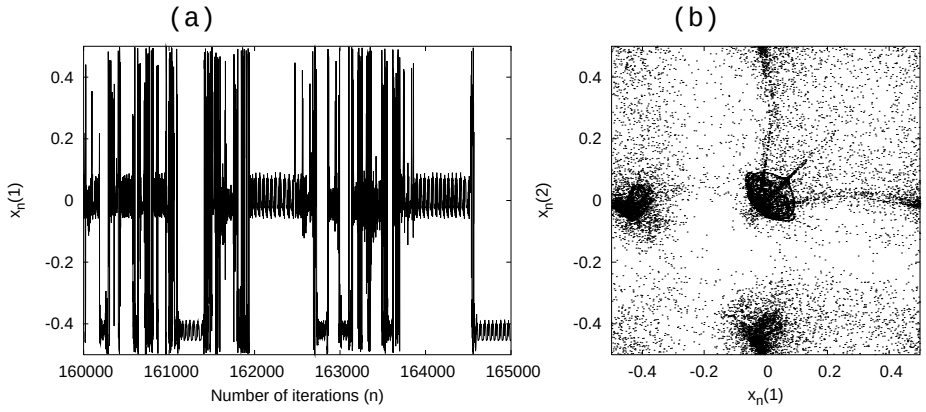

Figure 4: (a) Time series of chaotic itinerancy (CI). (b) Phase portrait in $x(1) - x(2)$ space of CI. This CI emerges after collapse of the tori shown in Fig.3. Such tori constitute an attractor ruin, where the orbits remain for a long time, carrying out a long-term trace. Here, $N = 5, \omega = 0.5$, and $\epsilon = 0.088858$.

randomly chosen parts of T1. In each test of stability, the strength of perturbation σ was fixed, and at each chosen part of T1, five directions were selected for the perturbations, each of which is taken along each axis of coordinate, and several other directions were also selected for confirmation. The torus T1 was judged to be completely stable under such perturbations with a fixed strength only if all the perturbed orbits are attracted to T1. The degree of instability was measured for each strength of perturbation by the probability $p(\sigma)$ of orbits being kicked out under such perturbations. From this computation, it is found that T1 is partially stable with respect to a perturbation of strength less than 0.003, because $\mathrm{p}(\sigma) > 0.995$ if $\sigma > 0.003$, and the strength below which the torus is completely stable is 2.0×10^{-5} because up to such a strength, the probability of escaping out of torus is zero. We regard the latter as the averaged "strength" [4] of the torus T1.

The complexity of a basin in the neighborhood of a torus can be expressed as the dependence of the attractor strength on the bifurcation parameter, i.e. the coupling strength ϵ. This dependence is shown in Fig. 6. Figure 6 (a) indicates that this dependence is roughly linear, but fine structures appear (Fig.6(b)), and they appear to be self-similar, reflecting a self-similar structure of the basin near the torus. It is observed that CI appears when this attractor strength becomes zero. At this critical point, the torus becomes unstable, though some stable manifolds of tori remain. For this reason, this torus is no longer a geometric attractor, but it is an attractor in Milnor's sense.

Each individual map has two indifferent fixed points, which are attractors in Milnor's sense. Each of these Milnor attractors is also an invariant set derived from symmetry of the coupled system, such as that responsible for the existence of the state in which all elements are synchronized. It is not, however, expected that these Milnor attractors possess a riddled basin. Because for riddling to exist, it is necessary that an invariant

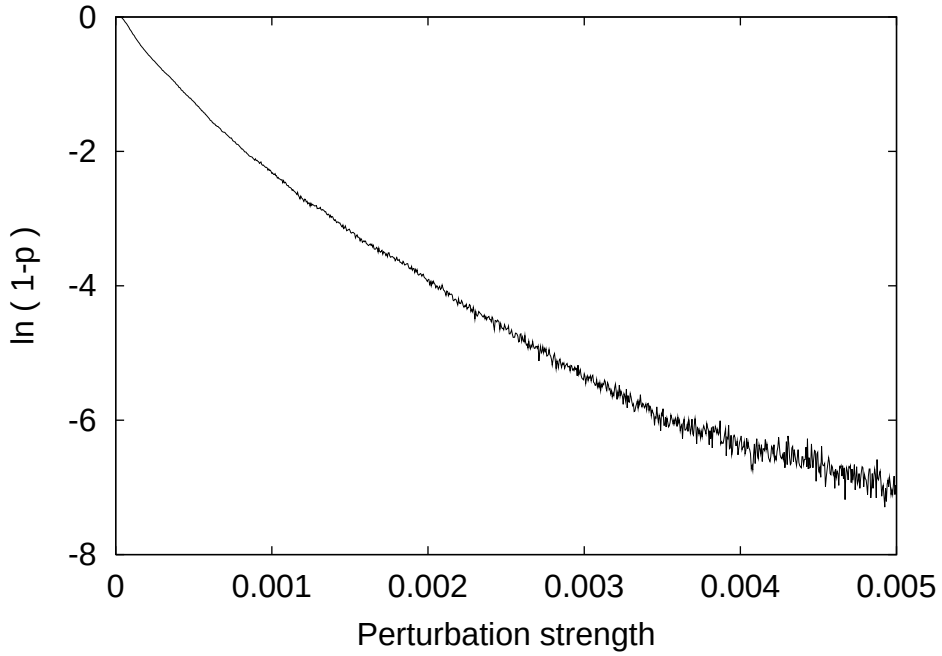

Figure 5: The "strength" of the torus T1. For a fixed strength of perturbation, the direction of the perturbation is chosen randomly. This is the sense in which the perturbation in this calculation is "random". A given point in the torus is considered to be a "kicked-out point" if at least one of 100 perturbations considered causes the orbit to leave the torus. By calculating the ratio of kicked-out points among the 30,000 randomly chosen points in the torus, the probability of an orbit being kicked out of the torus is estimated. The abscissa represents the strength of the perturbation and the ordinate the probability. Here, $N = 5, \omega = 0.5$, and $\epsilon = 0.08885$.

set has positive measure, whereas these Milnor attractors are simply fixed points (and, specifically, not a torus or a chaotic attractor). For this reason, in this model in order for CI to exist, it is necessary that there appears a torus or chaos, or a combination of these attractors. In the present case, every torus is generated by the interaction of these two indifferent fixed points. At the exact positions of these fixed points, the interaction term vanishes, and therefore a slight shift from these points brings about weak sinusoidal interactions. Incommensurate cycles give rise to tori, whose situation is easy to occur because of sinusoidal interactions.

We actually found CI, that appears, based on torus ruins. The above considerations derive another possibility of the appearance of CI in the present model, that is based on chaos as attractor ruins, as is seen in GCM [2]. Actually, we found such a case, which is discussed in the next section.

The other possibility can occur in the case of higher-dimensional dynamical systems, where the overall system motion is decomposed into two types of modes, high-frequency and low-frequency modes. If a certain combination of variables form high-frequency modes, which causes the motion to be erratic around indifferent fixed points of a sub-

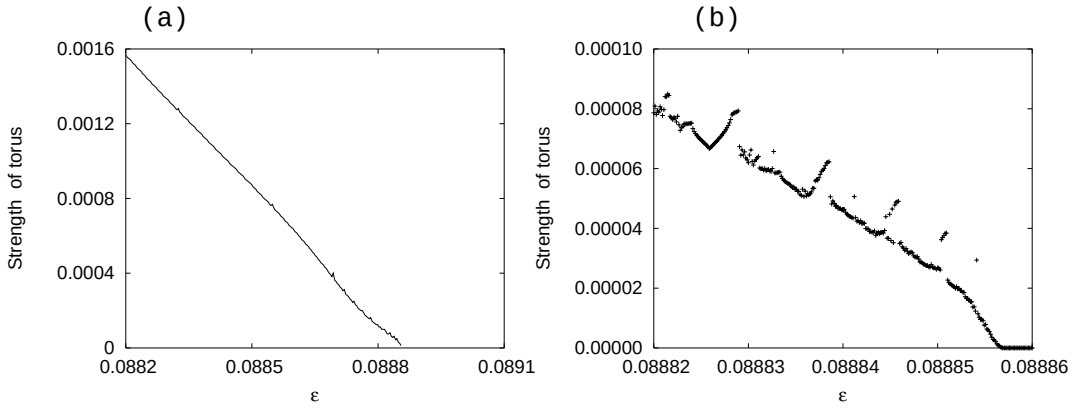

Figure 6: "Strength" of torus. The ordinate represents the minimum strength of the perturbation by which the orbit in the torus is kicked out. The abscissa represents the interaction strength ϵ. (a) An almost linear dependence is observed. (b)However, fine structure influenced by the fractal structure of the basin of the torus is clearly observed. Here, $N = 5, \omega = 0.5$.

system composed of variables that do not form high-frequency modes, then the motion around the indifferent fixed points can have positive measure. In such a case, the complex transitory dynamics between the "noisy" fixed points can appear as CI. We observed such CI generated from noisy fixed points in a non-equilibrium neural network model [14] and also in the present model with $N = 10$, $\omega = 0.5$ and $\epsilon = 0.037$, though the CI is transient in the latter case.

4 Observation of transient CI through local chaos

Chaotic itinerancy can also be generated from local chaos, as discussed in the previous section. In this section, we report several characteristics of this type of CI. A typical type of such CI was observed in the case $\omega = 1/2$ and $N = 10$, although this is transient behavior. One characteristic of this family of dynamical systems is that this CI coexists with other attractors, which form tori in this case. The ruin of the present CI results from local chaos that appears just before the CI. This local chaos possesses only one positive Lyapunov exponent and has dimension 3.38. In the transient CI, there are three positive exponents, and the Lyapunov dimension is in the range 4.5-5.0. Increasing the interaction parameter ϵ, global chaos appears. This global chaos emerges through the distortion of tori. In this regime beyond the critical point $\epsilon = 0.1$, the number of positive Lyapunov exponents is nine, and the Lyapunov dimension approaches to the full dimension, 10.

The local chaos are generated from two kinds of indifferent fixed points (point attractors in Milnor's sense). We found two types of local chaos, partially synchronized and desynchronized.

We often observe the curious behavior of a short-term switch between different types

of local chaos. There is the tendency that approximately fifty percent of the states of desynchronized chaos become synchronized through such a short-term excursion, but the reverse does not occur. Instead, the tracing phase of local chaos tends to be desynchronized after a long-term chaotic excursion. Altogether, we have observed the following progression: 'long-term global chaos' $\rightarrow$ 'desynchronized local chaos' $\rightarrow$ 'short-term global chaos' $\rightarrow$ 'synchronized local chaos' $\rightarrow$ 'long-term global chaos'.

In order to elucidate the details of the structure of phase space that are specific to the coexistence of the presently considered type of CI with tori, we further investigate the basin structure of tori. Tori exist in the neighborhood of the ruin of local chaos, and therefore a complex basin structure among tori is expected. We actually observe a riddled structure in almost all parts of phase space.

5 Distributions and ergodicity

The CI discussed in §2 can be decomposed into two distinct phases: the tracing phase of torus ruins and the chaotic transition phase. We investigated the characteristics of these phases. Several important questions arise in this investigation:

1. From where in the neighborhood of a torus does an orbit leave?
2. What is the distribution of the durations of chaotic transitions?
3. What is the distribution of the durations of orbits tracing torus ruins?
4. How do the Lyapunov exponents converge?
5. In relation to question 4, what about the ergodicity of the system?

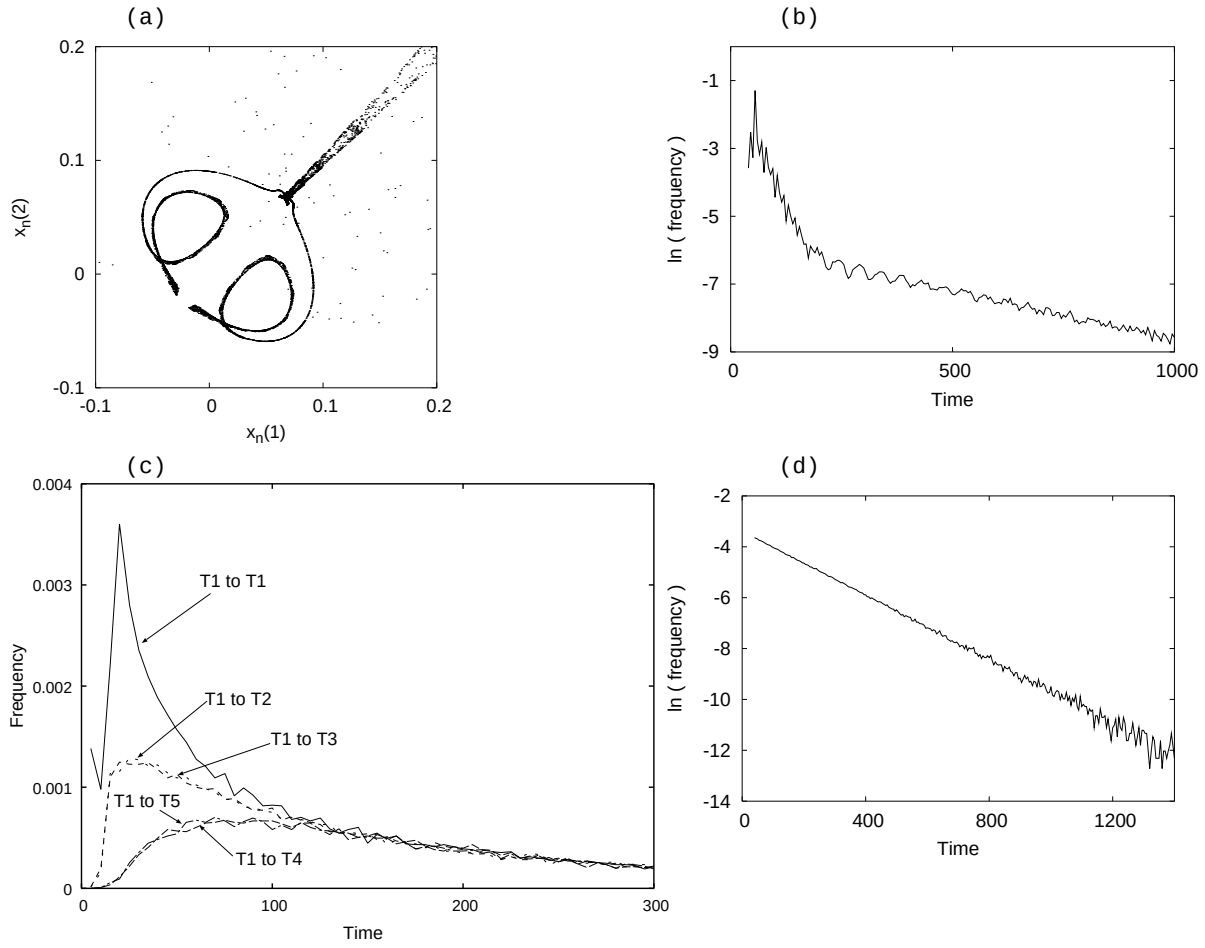

Figure 7: Structure of orbits and the statistics of the itinerancy. Here, $N = 5, \omega = 0.5$, and $\epsilon = 0.088858$. (a) Torus ruin of T1. Displayed here are a collection of the different orbits, each of which is that obtained for 30 time steps immediately preceding chaos. (b) Frequency distribution of the time in the attractor ruin. The ordinate is a log scale. A crossover of the form of the damping rate is seen. The damping rate is 0.0265 for $0 \leq n \leq 180$, and 0.00286 for $180 \leq n \leq 1,000$. (c) Frequency distribution of the time spent in chaotic transition when a transition from the torus T1 to the torus Tk ($k = 1 - 5$) occurs. The transition probability to each torus is the same for $n \geq 120$, but different for $n \leq 120$. (d) The frequency distribution of the time elapsed during chaotic transition. The ordinate is a log scale. The damping rate is 0.00631.

We attempt to give an answer to each question. The orbits that leave the ruin of the torus T1 are depicted in Fig.7 (a). We find that orbits can leave any part of the torus – except the places in the neighborhood of the diagonal part of T1 in $x(1)$-$x(2)$ space, and move into chaotic regions. The structure in the neighborhood of the diagonal part of attractor play a special role in the transition. Orbits cannot leave the lower side of the boundary of the torus along the diagonal part, but they can readily leave from upper boundary. This means that even tiny deviation from the synchronization of the variables $x(1)$ and $x(2)$ leads chaotic transition if amplitude of the variables is large enough. It is thus seen why orbits in the neighborhood of the diagonal part become chaotic only after a long time, while those that exist in the torus ruins become chaotic after a relatively short time.

The two types of orbits discussed above for transition determine the probability distribution, $P_T(n)$, of the residence times of orbits tracing torus ruins. As seen in Fig.4, the orbits that take a long time and those that take a short time to become chaotic contribute to the probability distribution in a different way. The transition for a short time gives unequal probabilities of the orbits approaching to other torus ruins, while that for a long time gives almost equal probabilities. The existence of these two types of orbits explains the presence of two regions in the distribution of the residence time in torus ruins, characterized by two different exponential forms, that is, the crossover . For short stays, we have the distribution $P_T(n) \propto exp(\lambda_1 n)$, where $\lambda_1 = -0.0265$, and for long stays, $P_T(n) \propto exp(\lambda_2 n)$, where $\lambda_2 = -0.00286$ (Fig. 7 (b)).

The crossover between these two characteristic forms of P_T may be related to the relation between the unequal distribution of times for short-term chaotic transitions between tori and the equal distribution of times for long-term transitions. These probability distributions $P_C(n)$ are shown in Fig.7 (c). This probability distribution of the chaotic transition time also exhibits an exponential form, $P_C(n) \propto exp(\lambda_3 n)$, where $\lambda_3 = -0.00631$ (see also Fig. 7 (d)). Exponential decay is also observed in higher-dimensional maps, for example with $N = 10$, where we have a similar crossover phenomenon in the distributions to that in the above P_T and the attractor ruins are those of local chaos.

We further investigated the Lyapunov exponents and found the very slow convergence of exponents. This implies that the temporal average is not practically useful. However, when we consider many orbits beginning from many different (randomly chosen) initial conditions and compute the average of the exponents over these orbits, the distribution of the exponents by this ensemble average converges rapidly. To clarify this point, we now give an example. Figure 8 depicts an instance of such slow convergence, where the frequencies of the time-dependent exponent with which the largest Lyapunov exponent evaluated at each value were tabulated over the following 100,000 time steps: (a) $n =$

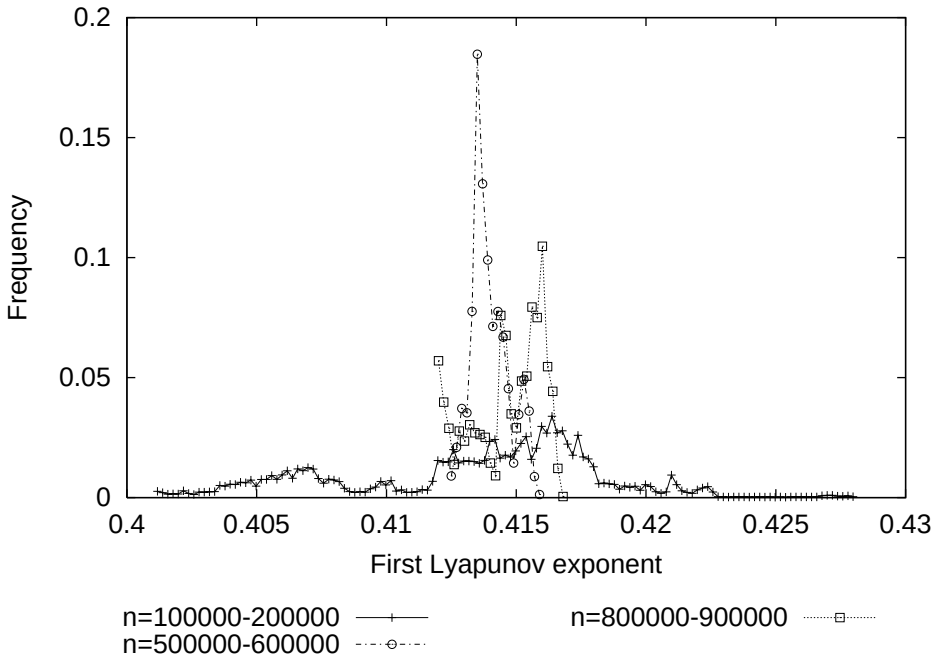

Figure 8: Fluctuations of the largest Lyapunov exponent. A long-term behavior of one selected orbit was observed for statistics. Normalization was performed for each five time steps. The frequency distribution of the time-dependent exponent during 100,000 steps for n = 100,000 - 200,000 (depicted by a solid line with crosses), n = 500,000 - 600,000 (by a dotted line with circles), and n = 800,000 - 900,000 (by a broken line with squares). The term "fluctuation of the Lyapunov exponent" is used in the sense that the time-dependent exponent that should converge to the Lyapunov exponent fluctuates and has a distribution of its values. This terminology is used in the text and also in the following figures. Here, only the largest Lyapunov exponent is depicted, but similar fluctuation is seen for the other exponents of the Lyapunov spectrum (see Fig. 12). Here, $N = 5, \omega = 0.5$, and $\epsilon = 0.088858$.

100,000-200,000, (b) n = 500,000-600,000, (c) n = 800,000-900,000. As seen in the figure, the distribution of the largest Lyapunov exponent gradually becomes sharp, but then it flattens out again, and this behavior is repeated. This characteristic of very slow convergence of the Lyapunov exponent in the long time average is also reflected by the time series of the average of the exponent up to some time and the scale of its variance. Figure 9 plots this average and variance in the cases of CI (in (a) and (b)) and usual chaotic behavior (in (c) and (d)). The chaotic behavior considered here is a global chaos for the case $N = 5, \omega = 0.5$, and $\epsilon = 0.12$.

In global chaotic behavior, the Lyapunov exponent converges rapidly, and its variance rapidly decays to zero, as shown in Figs. 9 (c) and (d). The satisfactorily small value $10^{-11} \sim 10^{-12}$, limited by the time used in the numerical computation. To further clarify the convergence in chaos, we calculated the same quantities in the case of the logistic map $x_{n+1} = 3.9x_n(1-x_n)$ and obtained results similar to those in Figs. 9 (c) and (d) (see Figs. 9 (e) and (f)). Contrastingly, in the case of the presently studied CI, the average value of the Lyapunov exponent fluctuates greatly in time, and the variance approaches some

finite value $\sim 10^{-9} \sim 10^{-8}$ and then fluctuates minutely about it, as shown in Figs. 9 (a) and (b). Thus, the statement that the existence of a non-zero variance is a good indication of the presence of CI seems to be reasonable, though we cannot deny the possibility that what we have observed here is an effect of the finite system size – that is, that the nonzero variance is due to the finite value of N. On the other hand, the following considerations guarantee the present assertion, independent of the system size, as far as CI occurs due to the appearance of Milnor attractors.

In the present study, we used the system size $N = 5$ that gives an intermediate level of two dynamical systems, CML and GCM, as indicated by $Q(5) = 1/2$. If we increase the system size, preserved a CML-type connection, then the effect of GCM becomes weak, and consequently CI becomes more difficult to be found. Actually, we found only transient CI in the case of $N = 10$. On the other hand, we also found a similar behavior of large fluctuations and extremely slow convergence of the Lyapunov exponents in GCM with logistic maps which was proposed as one typical model exhibiting CI. Kaneko [9] discussed in GCM with logistic maps a critical system size such that the Milnor attractors are dominant and then CI appears. Kaneko showed that in a wide class of GCM including asymmetric ones the critical size is 7 ± 2. This coincides with the condition of the appearance of attractor crowing. Actually, the system size $N = 6$ is obtained as the number of the smallest integer satisfying the inequality $(N-1)! > 2^N$, where $(N-1)!$ gives the order of the number of attractors and 2^N provides the phase space volume [9]. These facts indicate that this characteristic of Lyapunov exponents can give a universal index of the presence of CI, independent of an elementary individual model and its system size.

Furthermore, we calculated the index of the law that governs the convergence of large fluctuations of the averaged exponent [10, 11, 12]. Let $\lambda_1(t)$ be a time-dependent largest exponent and λ_1 be the converged value of the largest Lyapunov exponent. As seen from Fig. 10, the fluctuation of the average value $< (\lambda_1(t) - \lambda_1)^2 >$ damps extremely slowly. This quantity generally follows a power law $t^{-\alpha}$, where $0 < \alpha \leq 2$, if the time-dependent largest exponent calculated here reflects precisely an unstable component of tangent space. It is known that the relation $1 \leq \alpha \leq 2$ holds in the chaotic behavior with an exponential decay of correlations and $0 < \alpha < 1$ in the chaotic behavior with a power decay of correlations. The latter relation holds also in chaotic behavior of Hamiltonian systems because of the presence of tori in the chaotic sea (see, for example, Ref.[13]). We obtained in the present case $\alpha \sim 0.8$.

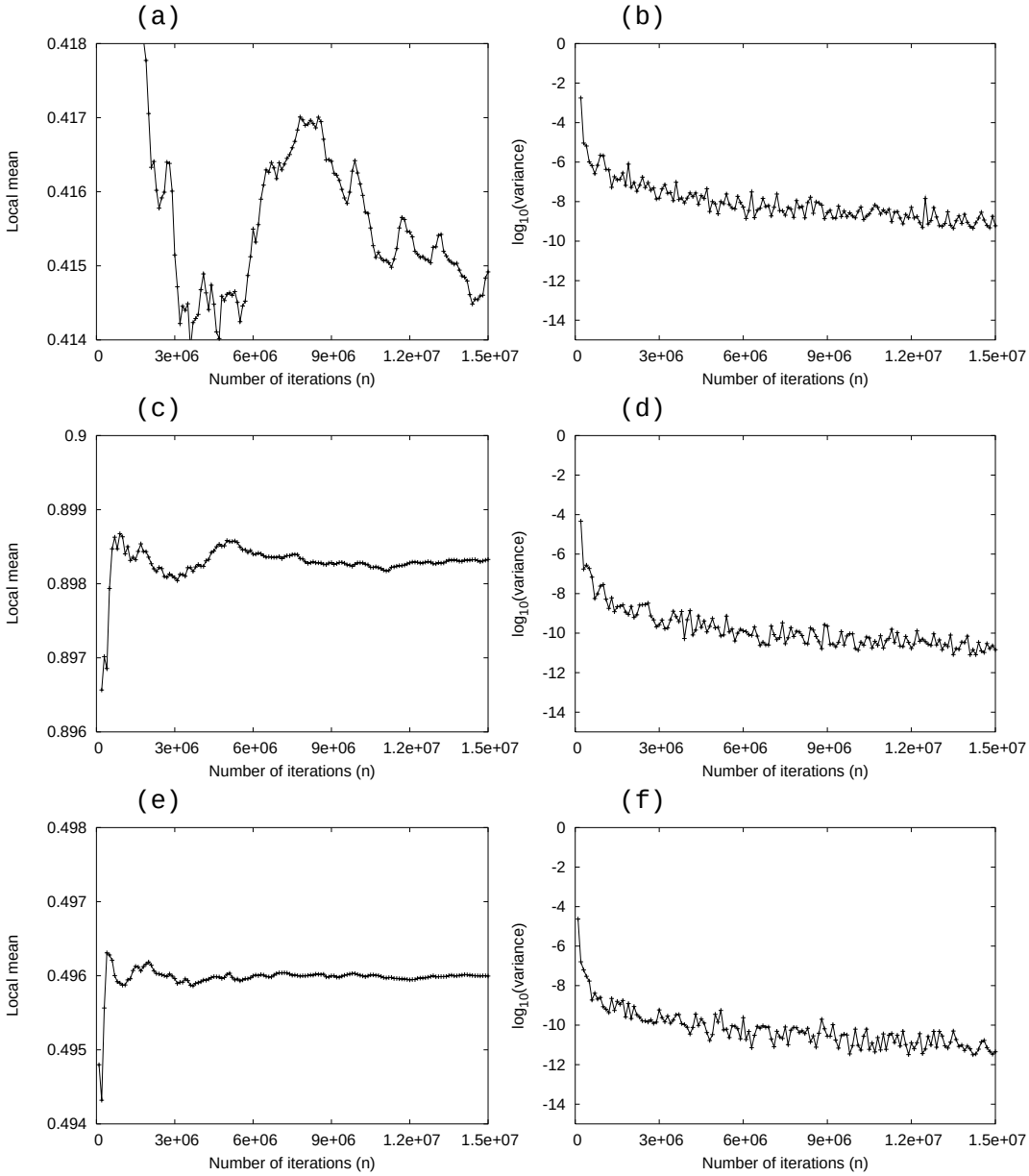

Figure 9: Comparison of the fluctuations of the largest Lyapunov exponent in the case of CI with that in the case of usual chaos. The averaged exponent and the variance over each 100,000 time steps is indicated by a cross. The temporal fluctuations of (a) the averaged largest exponent and (b) its variance in the case of CI, with $N = 5, \omega = 0.5$, and $\epsilon = 0.088858$. The temporal fluctuations of (c) the averaged largest exponent and (d) its variance in the case of global chaos, with $\omega = 0.5$, and $\epsilon = 0.12$. The corresponding quantities are shown in (e) and (f), respectively, in the case of logistic chaos obtained from the map $x_{n+1} = 3.9x_n(1 - x_n)$.

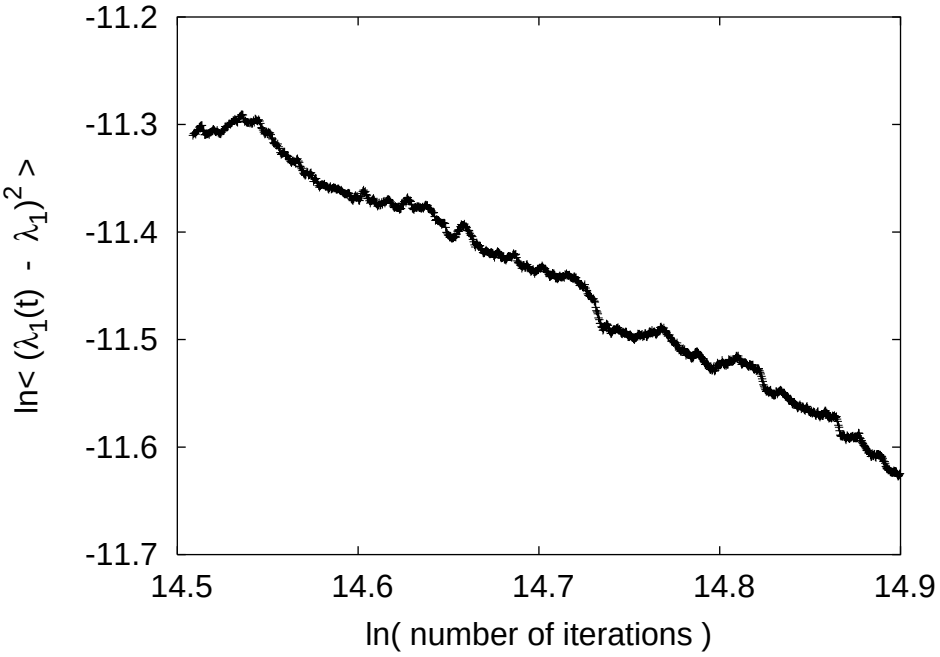

Figure 10: The fluctuation of the largest Lyapunov exponent at each time step that is defined as averaged square of the difference between the value of time-dependent largest exponent and the convergent value of the largest Lyapunov exponent decays in time as $t^{-\alpha}$, where $\alpha \sim 0.8$. The average was taken over five hundreds different initial conditions. The convergent value of the Lyapunov exponent was evaluated at n =30,000,000. The quantity $< (\lambda_1(t) - \lambda_1)^2 >$ needs a tough calculation, because of the difficulty of estimation of $lambda_1$ due to slow convergence. We believe the calculation of another quantity $< (\lambda_1(t) - \lambda_1(t-1))^2 >$ is much easier and gives more reliable estimation of the index. The reason why we used this quantity in this paper is just a comparison with theoretical values. The case considered is that of CI with $N = 5, \omega = 0.5$, and $\epsilon = 0.088858$.

Figure 11 shows the distribution of the largest Lyapunov exponent, evaluated at $n =$ 100,000. The averages were taken over 50,000 samples with randomly chosen initial conditions. This distribution converges to a certain smooth distribution. This indicates that the ensemble average of the largest Lyapunov exponent converges to a smooth distribution. When the number of time steps used in the evaluation of the Lyapunov exponent is increased further, the distribution of the ensemble average becomes sharper and sharper. This should converge to a delta function, but we observed (as mentioned above) that this convergence is extremely slow, behaving as $\sim n^{-0.8}$. From these considerations, we conclude that the system is ergodic in principle, but practically it is almost impossible to confirm this in a reasonable amount of time. Thus in any practically feasible observation, one would conclude that the system is chaotic but non-ergodic.

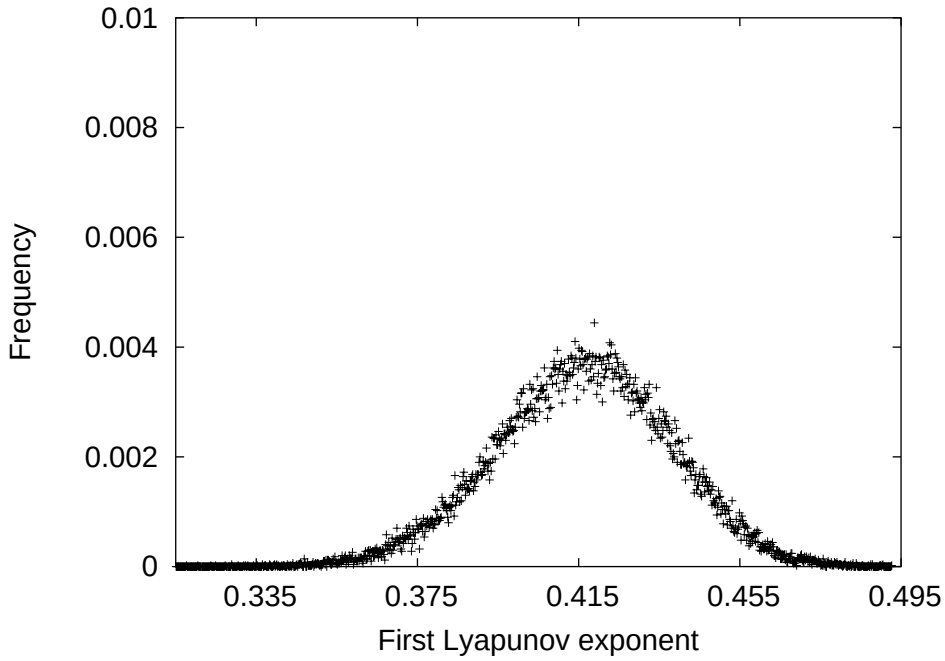

Figure 11: The distribution of the largest Lyapunov exponent evaluated over 100,000 steps. The average was taken over 50,000 samples.

The slow convergence of near-zero Lyapunov exponents has been investigated([16] and T. Sauer in this focus issue) as a possible indication of CI-like transition dynamics. Our study reveals that long-lasting and large fluctuations of the largest Lyapunov exponent is another such possible indication.

There are several possibilities for the mechanism underlying this type of slow convergence:

(a) The tangent space may not be spanned.

(b) The divergence and convergence of nearby orbits may be slower than exponential in time. For example, there may be of power-law forms.

(c) The other exponent(s) may fluctuate in such a way as to compensate for the fluctuation of the largest exponent.

In the case of (a) there is no convergence of all exponents, in the case (b) there is the fluctuation of only near-zero exponents, and the case of (c) can occur when the tangent space is degenerate. In order to clarify the mechanism underlying the presently considered very slow convergence, we also evaluated the convergence of other Lyapunov exponents (see Fig. 12). We found that in fact these exponents converge extremely slowly if at all, and hence we have the case (a).

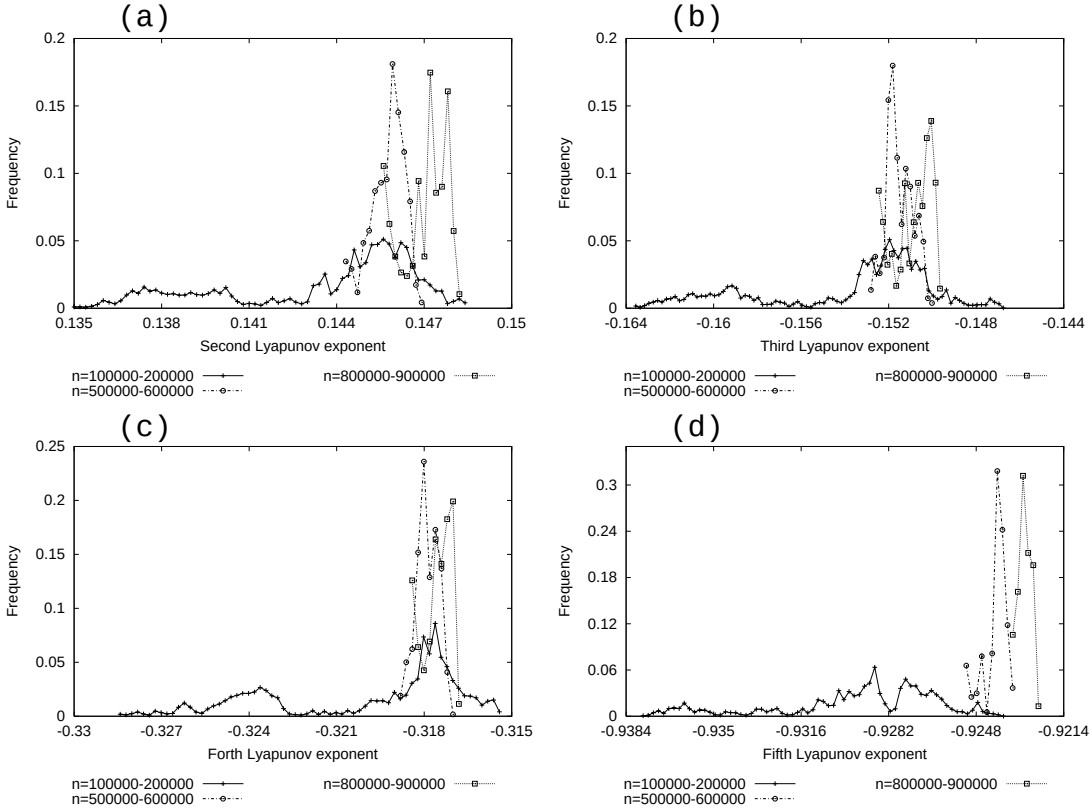

Figure 12: Fluctuations of other Lyapunov exponents than the largest one. (a) For the second, (b) the third, (c) the fourth and (d) the fifth Lyapunov exponent, respectively. For the notion of the figure, see the caption of Fig. 8.

6 Conclusion and Discussion

We observed chaotic itinerancy resulting from the coupling of Milnor attractors. Through the numerical studies, we conclude that the system with a size $N = 5$ characterized by $Q(5) = 1/2$, where the effects of CML and GCM are equal, still generates CI, but more CML-like systems (for instance, $N = 10$) generate only transient ones. In the present study, we considered a system consisting of coupled circle maps, whose uncoupled individual map produces Milnor attractors of the fixed point type. If these indifferent fixed points become an attractor ruin, only saddle connections can appear, and therefore it is not expected that CI will appear if there is no external noise. However, such a system may possess a similar phase space structure to the one of CI, as seen in noise-induced CI in non-equilibrium neural networks [17, 3, 14]. In such a case, the external noise can play the role of creating an invariant set that in some cases forms the basis of a riddled basin.

In the present model, CI is generated in a more complicated situation in which a torus or local chaos is that which creates an invariant set. All tori or local chaos can be identified by the system's symmetry, but in general, the generated transition path does

not necessarily possess this symmetry. For instance, the torus T2 can be obtained from the torus T1 by simply exchanging the variables $x(1)$ and $x(2)$, while T3 can be obtained from T2 by simply exchanging $x(2)$ and $x(3)$. Because of these symmetries, for every transition path from T1 to T2 there is an identical path from T2 to T3. However, it is not necessarily true that for every path from T1 to T2 there is an identical path from T1 to T3. Because of this type of asymmetry, in the CI existing in our system, the manner in which transitions are made between ruins of the different attractors depends on the initial conditions. For this reason, even though the system is ergodic, it appears to be non-ergodic. We have elucidated the reason that in any practically feasible observation of the system it will appear non-ergodic. We summarize our numerical results in the form of the following hypothesis.

Hypothesis

We conjecture that the apparent non-ergodic nature of the system resulting from the extremely slow convergence of the Lyapunov exponents is an indication of CI.

Chaotic itinerancy is universally observed in critical but, perhaps, structurally stable situations in high-dimensional dynamical systems. Also, in the dynamics of brain activity, a chaotic alternation between synchronized and desynchronized states in the visual cortex was found [18] and many studies have been made regarding the mechanism and the functional significance of this behavior. However, these have not yet been understood. We observed behavior similar to this type of chaotic alternation in the system studied here. This suggests that the present model may provide an appropriate dynamical interpretation of this curious behavior. Furthermore, other types of chaotic behavior of brain activity have been observed, including spatio-temporal chaos over a wide area of the olfactory system and the hippocampus [19] and perception drift [20]. Considering chaotic itinerancy and the mathematical description obtained in this paper as a model of non-stationary brain activity that observed in active animals and humans performing perceptual and cognitive tasks, it should be possible to investigate many types of such phenomena, including those mentioned above [15].

Acknowledgment

We would like to thank Takao Namiki for valuable discussions and useful comments on the manuscript. We express our special thanks to Motohiko Hatakeyama, Shigeru Kuroda and Satoru Tadokoro for valuable comments on the numerical calculations. This work is partially supported by a Grant-in-Aid (No.12210001) on Priority Area C, the Advanced Brain Science Project, from the Ministry of Education, Culture, Sports, Science, and Technology, Japan.

References

[1] K. Ikeda, K. Otsuka, and K. Matsumoto, Maxwell-Bloch turbulence, *Progress of Theoretical Physics, Supplement*, **99** (1989) 295-324.

[2] K. Kaneko, Clustering, coding, switching, hierarchical ordering, and control in network of chaotic elements. *Physica D* **41** (1990) 137-172.

[3] I. Tsuda, Chaotic itinerancy as a dynamical basis of Hermeneutics of brain and mind. *World Futures* **32** (1991) 167-185.

[4] K. Kaneko, Dominance of Milnor Attractors and noise-induced selection in a multiattractor system, *Phy. Rev. Lett.* **78** (1997) 2736-2739.

[5] J. Milnor, On the concept of attractor. *Communications in Mathematical Physics* **99** (1985) 177-195.

[6] K. Kaneko, ed., Chaos focus issue on coupled map lattices, *Chaos* **2** (1992) 279-.

[7] K. Kaneko, On the strength of attractors in a high-dimensional system: Milnor attractor network, robust global attraction, and noise-induced selection. *Physica D* **124** (1998) 322-344.

[8] K. T. Alligood, T. D. Sauer and J. A. Yorke, *Chaos* (Springer-Verlag New York, 1996).

[9] K.Kaneko, Dominance of Minlnor attractors in Globally Coupled Dynamical Systems with more than 7 +- 2 degrees of freedom. *Phys. Rev. E.* **66** (2002) 055201(R).

[10] H. Fujisaka, Statistical dynamics generated by fluctuations of local Lyapunov exponents, *Prog. Theor. Phys.* **70** (1983)1264-1275

[11] Y. Takahashi and Y. Oono, Towards the statistical mechanics of chaos, *Prog. Theor. Phys.* **71** (1984) 851-854.

[12] H. Mori, H. Hata, T. Horita and T. Kobayashi, Statistical mechanics of dynamical systems, *Prog. Theor. Phys. Suppl* **99** (1989) 1-63.

[13] Y. Aizawa, Symbolic Dynamics Approach to the Two-Dimensional Chaos in Area-Preserving Maps : A Fractal Geometrical Model. *Prog. Theor. Phys.* **71** (1984) 1419-1421.

[14] I. Tsuda, Dynamic link of memories–chaotic memory map in non-equilibrium neural networks. *Neural Networks* **5** (1992) 313-326.

[15] I. Tsuda, Toward an interpretation of dynamic neural activity in terms of chaotic dynamical systems, Behavioral and Brain Sciences, **24(5)** (2001) 793-847.

[16] S. Dawson, C. Grebogi, T. Sauer, and J. A. Yorke, Obstructions to Shadowing When a Lyapunov Exponent Fluctuates about Zero. *Physical Review Letters*, **73(14)** (1994) 1927-1930; T. Sauer, The effect of chaotic itinerancy on computer simulations. *Abstracts for SIAM Pacific Rim Dynamical Systems Conference*, August 9-13, 2000, Maui, Hawaii: p. 51.

[17] I. Tsuda, E. Körner and H. Shimizu, Memory dynamics in asynchronous neural networks. *Progress of Theoretical Physics* **78** (1987) 51-71.

[18] C. Gray, A. K. Engel, P. König, and W. Singer, Synchronization of oscillatory neuronal responses in cat striate cortex: Temporal properties, *Visual Neuroscience* **8** (1992) 337-347.

[19] L. Kay, L. R. Lancaster, and W. J. Freeman, Reafference and attractors in the olfactory system during odor recognition. *International Journal of Neural Systems* **7** (1996) 489-495.

[20] W. J. Freeman, *Societies of Brains – A Study in the Neuroscience of Love and Hate.* Lawrence Erlbaum Associates, Inc., Hillsdale, 1995; W. J. Freeman, *How Brains Make up Their Minds.* Weidenfeld & Nicolson, London, 1999.